Available online at www.sciencedirect.com
SCIENCE DIRECT®
Journal of Solid State Chemistry 179 (2006) 775–792
JOURNAL OF SOLID STATE CHEMISTRY
www.elsevier.com/locate/jssc

Composition dependence of the structural chemistry and magnetism of $Ca_{2.5}Sr_{0.5}(Ga,Co)_{1+x}Mn_{2-x}O_8$

Mathieu Allix[a], Peter D. Battle[b,*], Philip P.C. Frampton[b], Matthew J. Rosseinsky[a], Rocío Ruiz-Bustos[b]

[a]*Department of Chemistry, University of Liverpool, Liverpool L69 7ZD, UK*
[b]*Inorganic Chemistry Laboratory, Oxford University, South Parks Road, Oxford OX1 3QR, UK*

Received 14 October 2005; received in revised form 23 November 2005; accepted 23 November 2005
Available online 10 January 2006

Abstract

Polycrystalline samples of bilayered brownmillerite-like $Ca_{2.5}Sr_{0.5}GaCo_{0.15}Mn_{1.85}O_8$ and $Ca_{2.5}Sr_{0.5}Ga_{1.2}Mn_{1.8}O_8$ have been prepared and characterised by magnetometry and neutron diffraction over a wide temperature range. The structural chemistry and magnetic properties are compared to those of $Ca_{2.5}Sr_{0.5}GaMn_2O_8$. Ga enrichment has a significant effect on the former but not on the latter, whereas changes in both occur when paramagnetic Co^{3+} cations enter the parent phase on the 4-coordinate sites. The coupling between the environment around the 4-coordinate cations and the transition to an antiferromagnetic ordered state that was observed in $Ca_{2.5}Sr_{0.5}GaMn_2O_8$ is not apparent in the cation-substituted compositions, although both show long-range antiferromagnetic order at low temperatures.

Keywords: Brownmillerite

1. Introduction

We have previously shown [1,2] that the mixed-valence compound $Ca_{2.5}Sr_{0.5}GaMn_2O_8$ is an anion-deficient perovskite in which the vacant anion sites order so as to create a structure in which perovskite bilayers consisting of corner-sharing MnO_6 octahedra are isolated from each other by a single layer of GaO_4 tetrahedra. The electronic properties of this phase are highly relevant to the debate concerning spin, charge and orbital ordering which has grown out of recent attempts to optimise the magnetotransport properties of perovskite-related Mn oxides [3–8]. We have argued that the low-temperature antiferromagnetic structure of this compound is best rationalised by assuming that, on cooling, one-dimensional ordering of Mn^{3+} and Mn^{4+} cations occurs in a direction perpendicular to the perovskite layers, although, surprisingly, the major structural change associated with the onset of long-range magnetic order involves the Ga–O bonds which lie almost parallel to the layers. It is remarkable that the chemical bonding around a diamagnetic cation should show such a strong response to an electronic phase transition in a complex transition-metal oxide. As formulated above, this compound contains a 1:1 ratio of Mn^{3+} and Mn^{4+}, and one aspect of our recent research programme has involved attempts to vary this ratio by making appropriate chemical substitutions, for example, Ln^{3+} (Ln = La, Nd, Y) for Sr^{2+}. However, the parent compound has proved to be remarkably resistant to this type of approach and we have therefore attempted to vary the number of d electrons in the system by replacing Mn with other transition metals. We describe below the synthesis and characterisation of $Ca_{2.5}Sr_{0.5}GaCo_{0.15}Mn_{1.85}O_8$. We shall show that although the average crystal structure of this composition bears a strong resemblance to that of $Ca_{2.5}Sr_{0.5}GaMn_2O_8$ there are a number of differences that are important in the determination of magnetic behaviour. These differences include the transfer of some diamagnetic Ga^{3+} cations to the 6-coordinate site and the presence of magnetic Co

*Corresponding author. Fax: +44 1865 272690.
E-mail address: peter.battle@chem.ox.ac.uk (P.D. Battle).

0022-4596/$ - see front matter © 2005 Elsevier Inc. All rights reserved.
doi:10.1016/j.jssc.2005.11.037

cations on the tetrahedral sites. In order to determine the relative importance of the structural changes we have also prepared and characterised $Ca_{2.5}Sr_{0.5}Ga_{1.2}Mn_{1.8}O_8$ as a reference material. Interestingly, neither substituted phase shows the complex temperature-dependent structural chemistry seen in the parent compound, although both adopt the same antiferromagnetic structure at low temperatures.

2. Experimental section

A polycrystalline sample (~2 g) of $Ca_{2.5}Sr_{0.5}GaCo_{0.15}Mn_{1.85}O_8$ was synthesised by heating in air a well-ground, stoichiometric mixture of $CaCO_3$, $SrCO_3$, Ga_2O_3, Co_3O_4 and MnO_2 contained in an alumina crucible. The pelletised mixture was heated for a total of 8 days at 1000 °C and then for 8 days at 1050 °C, the reactants being remixed and repelletised at frequent intervals. A sample of $Ca_{2.5}Sr_{0.5}Ga_{1.2}Mn_{1.8}O_8$ was prepared in a similar manner, with an initial 24 h heating at 1000 °C being followed by a total of 240 h at 1150 °C. The reactions were deemed to be complete when the X-ray powder diffraction patterns of the products did not change on further heating. Data suitable for structure refinement by Rietveld profile analysis were collected at room temperature on a Siemens D5000 diffractometer operating with Cu $K\alpha_1$ radiation in Bragg-Brentano geometry over the angular range $5<2\theta(\text{deg})<120$ with a step size $\Delta 2\theta = 0.02^\circ$. Neutron diffraction data were subsequently collected over the d-spacing range $0.6<d(\text{Å})<6$ on the time-of-flight powder diffractometer GEM at ISIS, Rutherford Appleton Laboratory. Data were collected on $Ca_{2.5}Sr_{0.5}GaCo_{0.15}Mn_{1.85}O_8$ at temperatures of 10, 300, 673, and 873 K, and at 10 K intervals over the range $40 \leqslant T(\text{K}) \leqslant 230$. In the case of $Ca_{2.5}Sr_{0.5}Ga_{1.2}Mn_{1.8}O_8$ data were collected at intervals of 10 K over the temperature range $60 \leqslant T(\text{K}) \leqslant 270$. The raw data were corrected for absorption effects using the Ariel software provided by ISIS. An additional data set was collected on $Ca_{2.5}Sr_{0.5}Ga_{1.2}Mn_{1.8}O_8$ at 10 K using the diffractometer D2b at ILL Grenoble.

The samples were also studied by electron microscopy. After being crushed in ethanol, the small crystallites in suspension were deposited onto a holey carbon film, supported by a copper grid. The electron diffraction (ED) study was carried out with a JEOL 2000FX electron microscope equipped with an EDAX analyser. The chemical homogeneity was verified by energy dispersive spectroscopy (EDS) analysis during the ED study. High-resolution electron microscopy (HREM) was performed with a JEOL 2000EX microscope with a point resolution of 2.4 Å (accelerating voltage = 200 kV). HREM image simulation was performed using EMS Bloch wave calculations [9], varying the focus values and crystal thickness and using the atomic positions obtained from the analysis of neutron powder diffraction data.

The magnetic behaviour of the samples was studied using a Quantum Design MPMS SQUID magnetometer. The sample magnetisation was measured in a field of 100 Oe on warming through the temperature range $5 \leqslant T(\text{K}) \leqslant 300$ after cooling the sample both in the measuring field (field cooling—FC) and in the absence of an applied field (zero-field cooling—ZFC). The magnetisation was also measured as a function of field ($-50 \leqslant H(\text{kOe}) \leqslant 50$) at selected temperatures: 5, 60, 100, 200 and 250 K in the case of $Ca_{2.5}Sr_{0.5}GaCo_{0.15}Mn_{1.85}O_8$ and 5, 100, 200 and 300 K in the case of $Ca_{2.5}Sr_{0.5}Ga_{1.2}Mn_{1.8}O_8$. Data were collected in decreasing and increasing fields after cooling from the paramagnetic phase to the chosen temperature in a field of 50 kOe.

3. Results

3.1. $Ca_{2.5}Sr_{0.5}GaCo_{0.15}Mn_{1.85}O_8$

Profile analysis, performed using the GSAS program suite [10], of the X-ray powder diffraction pattern of the reaction product suggested that it was a monophasic sample of the target material. This was true for all lightly doped compositions ($x \leqslant 0.3$) synthesised in the system $Ca_{2.5}Sr_{0.5}Mn_{2-x}Co_xGaO_8$, but magnetic data suggested that an impurity, undetected by X-ray diffraction, was present in the composition range $0.2 \leqslant x \leqslant 0.3$. The X-ray diffraction patterns of samples for which $x > 0.3$ revealed the presence of a single-layer brownmillerite impurity. These observations, together with our desire to work on a pure sample, caused us to focus on a sample having $x = 0.15$. Analysis of this material by EDS found no evidence of inhomogeneity and gave a metal composition of $Ca_{2.39}Sr_{0.51}$ $Ga_{1.01}$ $Co_{0.15}Mn_{1.92}$ ($\pm 5\%$). Ten crystallites showing a high degree of crystallinity were studied in detail by ED. A reciprocal lattice was constructed from two of them, and the diffraction patterns taken along various zone axes (Fig. 1) could be indexed, as anticipated, in space group $Pcm2_1$ with $a \sim 5.4$ Å, $b \sim 11.4$ Å and $c \sim 5.3$ Å. Lattice images could be well matched (Fig. 2) to computer simulations based on the structural parameters derived from our neutron diffraction experiments. There was no evidence in either the diffraction patterns or the images for the presence of microdomains showing a doubling of the unit cell along [010]. Such a doubling was observed in the case of the Co-free parent compound and was attributed to an ordering of the orientation of the GaO_4 tetrahedra.

The temperature dependence of the molar magnetic susceptibility of $Ca_{2.5}Sr_{0.5}GaCo_{0.15}Mn_{1.85}O_8$ is shown in Fig. 3. The data show a local maximum at 155 K, and hysteresis is apparent between the FC and ZFC data below this temperature. The ZFC, but not the FC, data show a second turning point at 8 K. The data in the temperature range $235 \leqslant T(\text{K}) \leqslant 300$ could be fitted to a Curie–Weiss Law with $C_m = 7.8(3)$ emu and $\theta = -238(1)$ K. This value of the Curie constant corresponds to a mean effective magnetic moment $\mu_{\text{eff}} = 5.6\,\mu_B$ per cation, assuming that there are two magnetic cations per formula unit. Fig. 4

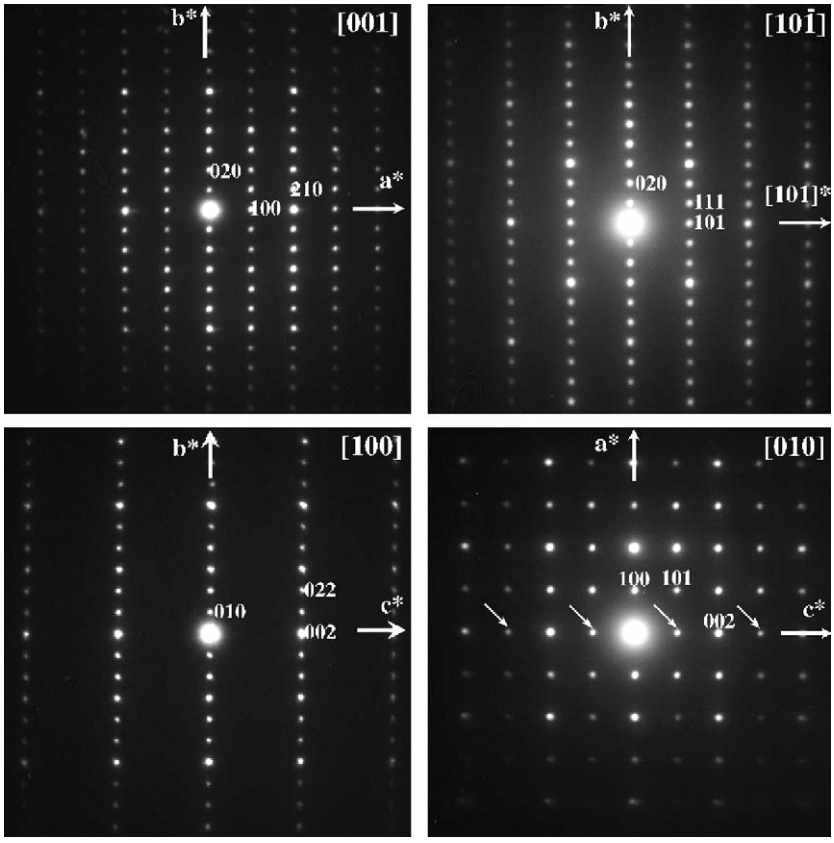

Fig. 1. Typical experimental [001], [10$\bar{1}$], [100] and [010] electron diffraction patterns of $Ca_{2.5}Sr_{0.5}GaCo_{0.15}Mn_{1.85}O_8$, indexed using a $5.4 \times 11.4 \times 5.3$ Å unit cell. The patterns taken from $Ca_{2.5}Sr_{0.5}Ga_{1.2}Mn_{1.8}O_8$ are similar. The small white arrows on the [010] oriented pattern indicate reflections attributable to double diffraction.

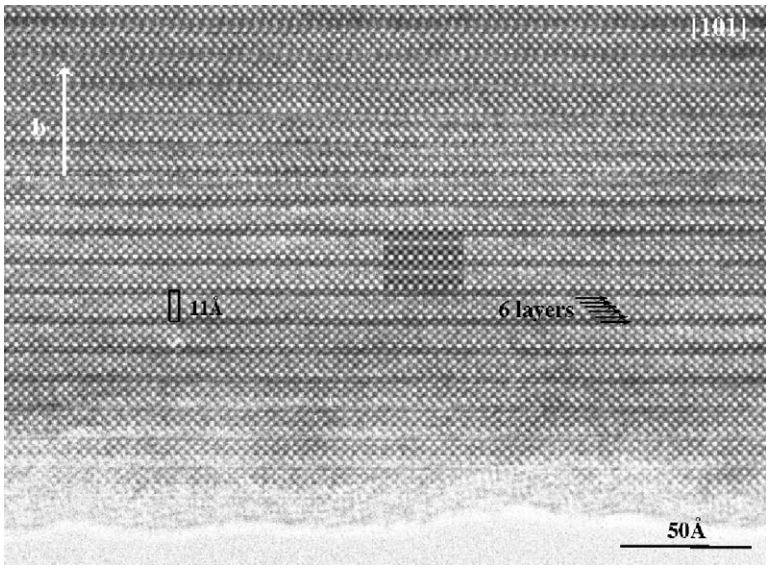

Fig. 2. HREM image of $Ca_{2.5}Sr_{0.5}GaCo_{0.15}Mn_{1.85}O_8$ recorded along [101], the simulated image is embedded (focus value 10 nm and thickness of the crystal 40 Å). A unit cell containing 6 cation layers (Ca–Ga–Ca–Mn–Sr–Mn) is outlined.

shows the field dependence of the magnetisation, $M(H)$, at 5, 60, and 200 K. Plots of the data collected at all temperatures above 5 K pass through the origin and show no significant hysteresis. The $M(H)$ curve collected at 5 K is shifted along the positive magnetisation axis and shows a finite width.

A detailed structural study of $Ca_{2.5}Sr_{0.5}GaCo_{0.15}Mn_{1.85}O_8$ was carried out using neutron diffraction data.

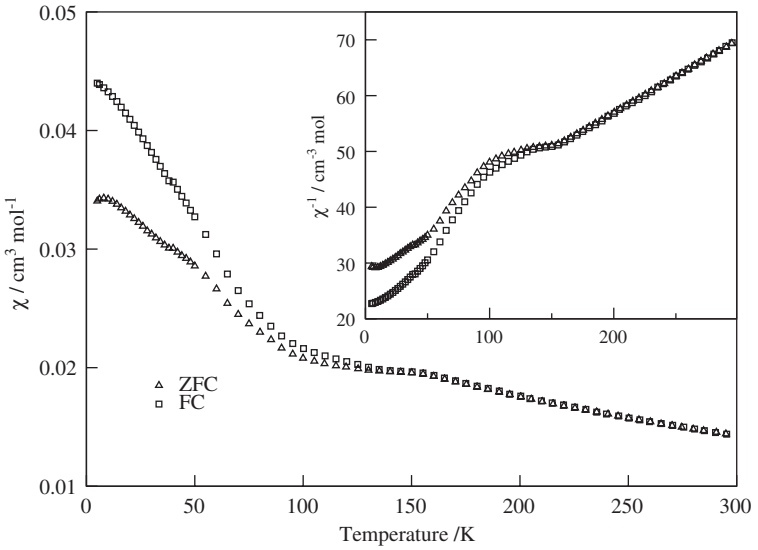

Fig. 3. Temperature dependence of the molar magnetic susceptibility of $Ca_{2.5}Sr_{0.5}GaCo_{0.15}Mn_{1.85}O_8$ measured in 100 Oe after zero-field cooling (ZFC) and field cooling (FC).

All profile analyses were carried out using the GSAS program suite. A convolution of Ikeda-Carpenter and pseudo-Voight functions was used to model the peak profile and a shifted Chebyshev polynomial was used to model the background. Each atomic position was assigned an isotropic displacement parameter. The data analysis proved to be much more complex than in the case of $Ca_{2.5}Sr_{0.5}GaMn_2O_8$. Although the diffraction patterns could again be indexed in the orthorhombic space group $Pcm2_1$, it became apparent that at high temperatures there was considerable disorder amongst the oxide ions (O1) within the layers of tetrahedra. In order to model this it was necessary either to accept an abnormally high value for the refined isotropic atomic displacement parameter ($u = 0.0122(8)$ Å^2 at 300 K, cf. $u = 0.0052(5)$ for O2) or to disorder the atom over two sites related by the mirror plane at $y = 0$. At the lowest temperatures studied there was less evidence for disorder, and the displacement parameter refined to a reasonable value ($u = 0.0073(8)$ Å^2 at 10 K, cf. $u = 0.0040(5)$ for O2). After several trial refinements we chose a disordered model for the structure at high temperatures and an ordered model at low temperatures. The data sets collected at intermediate temperatures were analysed using both models, and the quality of the analyses were always comparable. We can thus describe the O1 site as showing a decreasing degree of static disorder on cooling, although we are unable to identify a temperature at which the disorder can be said to disappear. A full set of refinements using both models was carried out in order to ensure that none of the other conclusions drawn from this study are dependent on the description of the O1 site. Our initial refinements were carried out with the assumption that the Co cations substitute for Mn cations within the perovskite bilayers. However, when a fraction of the Co atoms were allowed to exchange sites with an equal number of Ga atoms the number of Co atoms remaining on the octahedral site was insignificant ($<3\sigma$) and consequently in our final refinements of the structure at all temperatures the Co atoms were located on only the tetrahedral site. Our description of this site thus involves both a random 15:85 distribution of two cations and, at least at high temperatures, a disordered arrangement of the coordinating anions. However, there was no evidence in difference-Fourier maps for the presence of more than four anions around the site. The 6-coordinate sites are occupied by a random distribution of Mn and Ga in a ratio 1.85:0.15. The displacement parameter of the 6-coordinate site refined to a negative value in this model and was subsequently fixed at zero. This effect has been seen in other refinements of Mn-containing compounds [11,12] and ascribed to an inadequate absorption correction. In the present case the limitations of the model used to describe the Mn^{3+}/Mn^{4+}/Ga disorder around the 6-coordinate sites will also be a factor. The ordering of the Ca and Sr atoms was shown in test refinements to be the same as that observed in the undoped compound, with a 1:1 random distribution of Ca and Sr over the sites within the perovskite bilayers and only Ca atoms occupying the sites between the bilayers and the tetrahedral layer. The distribution of these two elements was held constant in the refinements detailed below. The structural model established in these preliminary refinements was able to account for all the neutron diffraction data collected in the temperature range $160 \leqslant T(\mathrm{K}) \leqslant 873$. The structural parameters resulting from the analysis of the data collected at 300 K are listed in Table 1; the atom-numbering scheme is defined in Fig. 5 which shows the local coordination at the octahedral and tetrahedral sites. The displacement parameters associated with the tetrahedral and O1 sites in the disordered model refined to values

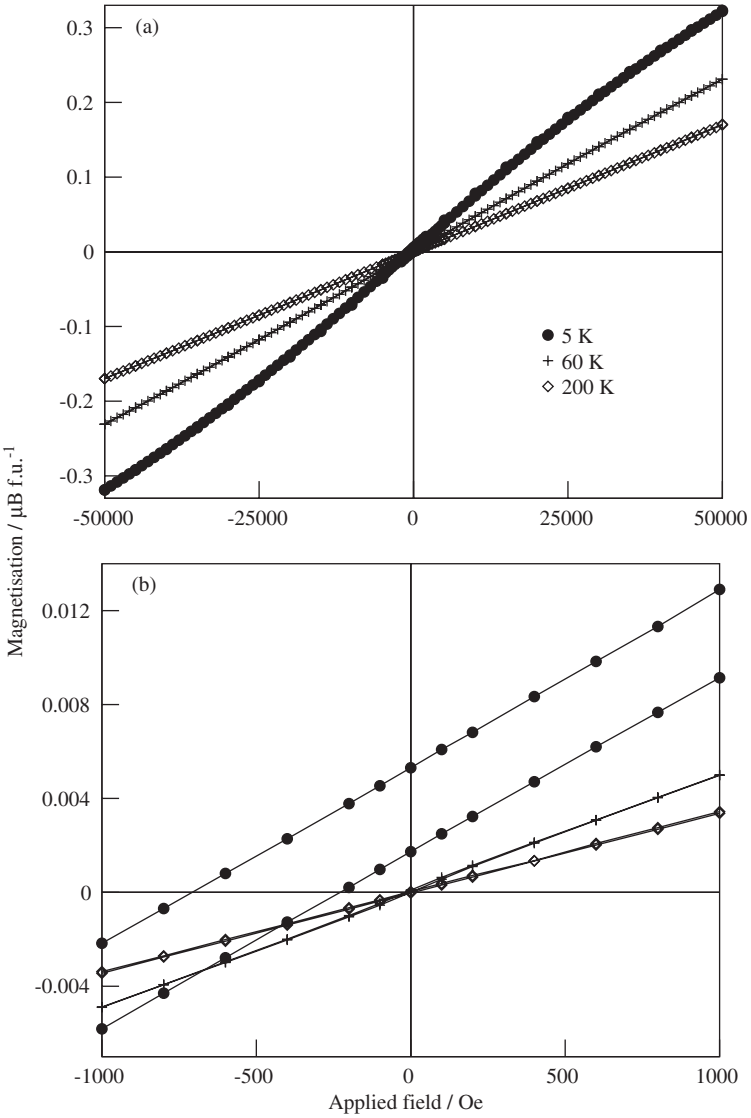

Fig. 4. Field dependence of the magnetisation of $Ca_{2.5}Sr_{0.5}GaCo_{0.15}Mn_{1.85}O_8$ at 5, 60 and 200 K.

which are negative, but not significantly so when considered in the light of the standard deviations.

The high *d*-spacing region of the data set collected at 10 K contained Bragg peaks that were not observed in the data sets described above. These peaks were apparently consistent with the adoption of the same antiferromagnetic spin-ordering pattern as was observed [1] in $Ca_{2.5}Sr_{0.5}GaMn_2O_8$. The atomic parameters resulting from simultaneous refinement of the low-temperature crystal and magnetic structures of the Co-doped phase are also listed in Table 1. The magnetic moment on the 6-coordinate site refined to a value of 2.453(6) μ_B per Mn cation. In the final stages of our data analysis a magnetic moment was introduced on the 4-coordinate sites occupied by Co. This produced a noticeable improvement in the profile fitting for $d > 3.5$ Å and resulted in an ordered moment of 1.70(7) μ_B per Co, aligned antiparallel to the Mn moments in the same [010] chain. The observation of a magnetic moment on the 4-coordinate sites of course reinforces our conclusion concerning the Co/Ga site distribution. The magnetic structure is drawn in Fig. 6. The displacement parameter at the Ca 4*c* site becomes significantly negative on cooling to 10 K; we ascribe this deficiency in our description of the structure to correlations between parameters introduced by the appearance of Q-dependent magnetic scattering in the data.

The data collected in the temperature region $40 \leqslant T(K) \leqslant 230$ allow us to study the evolution of both the crystal and magnetic structures with temperature. Fig. 7 shows the temperature dependence of the ordered magnetic moment at the 6- and 4-coordinate sites. Magnetic scattering was clearly present in the data collected at 150 K, but not in those taken at 160 K (Fig. 8); attempts to include an ordered magnetic moment

Table 1
Structural parameters of $Ca_{2.5}Sr_{0.5}GaCo_{0.15}Mn_{1.85}O_8$ as a function of temperature

	300 K ordered	300 K disordered	10 K ordered
a (Å)	5.44727(6)	5.44727(6)	5.43587(7)
b (Å)	11.3197(1)	11.3198(1)	11.3134(1)
c (Å)	5.31012(6)	5.31009(6)	5.29769(7)
Volume (Å^3)	327.43(1)	327.43(1)	325.80(1)
Combined R_{wp}	2.78%	2.78%	3.17%
Ca 4*c*			
x	0.2256(3)	0.2246(3)	0.2237(3)
y	0.1896(1)	0.1895(1)	0.1897(1)
z	0.5115(9)	0.5128(9)	0.517(1)
U_{iso} (Å^2)	0.0002(4)	0.0013(4)	−0.0026(4)
Ca/Sr 2*b*			
x	0.2400(3)	0.2414(3)	0.2395(4)
z	0.4986(9)	0.4989(9)	0.495(1)
U_{iso} (Å^2)	0.0094(5)	0.0083(5)	0.0070(6)
Octahedral 4*c*			
x	0.2553(5)	0.2555(5)	0.2541(7)
y	0.3302(2)	0.3298(2)	0.331(2)
z	0	0	0
U_{iso} (Å^2)	0	0	0
Tetrahedral 2*a*			
x	0.3211(3)	0.3222(3)	0.3223(3)
z	0.0487(8)	0.0530(8)	0.054(1)
U_{iso} (Å^2)	0.0011(6)	−0.0001(6)	−0.0010(7)
O1 2*a* (4*c*)			
x	0.3670(3)	0.3678(3)	0.3661(3)
y	0	0.0181(3)	0
z	0.4061(8)	0.4072(8)	0.4092(9)
U_{iso} (Å^2)	0.0122(8)	−0.0018(9)	0.0073(8)
O2 2*b*			
x	0.3016(3)	0.3678(3)	0.3035(3)
z	0.000(1)	0.001(1)	0.001(1)
U_{iso} (Å^2)	0.0052(5)	0.0071(5)	0.0040(5)
O3 4*c*			
x	0.1873(2)	0.1872(2)	0.1874(2)
y	0.1429(1)	0.1427(1)	0.1426(1)
z	−0.022(1)	−0.019(1)	−0.018(1)
U_{iso} (Å^2)	0.0073(4)	0.0104(4)	0.0078(4)
O4 4*c*			
x	−0.0029(3)	−0.0017(3)	−0.0059(3)
y	0.3425(1)	0.3425(1)	0.3421(1)
z	0.247(1)	0.248(1)	0.244(1)
U_{iso} (Å^2)	0.0035(3)	0.0040(3)	0.0007(3)
O5 4*c*			
x	0.4930(3)	0.4929(3)	0.4905(3)
y	0.3069(1)	0.3072(1)	0.3070(1)
z	0.256(1)	0.258(1)	0.261(1)
U_{iso} (Å^2)	0.0048(4)	0.0051(4)	0.0008(4)

in the analysis of the latter resulted in unstable refinements. The unit cell parameters a and c show (Fig. 9) no anomaly at 150 K, but parameter b increases with decreasing temperature for $80 \leqslant T(K) \leqslant 150$; the unit cell volume decreases on cooling through this temperature range. The bond lengths around the 6-coordinate site do not show any significant change at the Néel temperature, and neither does the Mn–O2–Mn bond angle (Fig. 10). Finally, Fig. 11 shows that the bond lengths around the 4-coordinate site do not respond to the magnetic phase transition. Fig. 11 shows two sets of curves in order to represent the results of analyses using a split-site description of O1 and of those in which a single site was used. Although there is a systematic displacement of the two curves, neither shows a marked temperature dependence of the bond lengths.

3.2. $Ca_{2.5}Sr_{0.5}Ga_{1.2}Mn_{1.8}O_8$

X-ray powder diffraction data indicated that we had prepared a single-phase sample of $Ca_{2.5}Sr_{0.5}Ga_{1.2}Mn_{1.8}O_8$; attempts to introduce a higher Ga content resulted in reaction products that clearly contained a perovskite impurity. EDS analysis of 20 crystallites of this material found no evidence of inhomogeneity and gave a metal composition of $Ca_{2.49}Sr_{0.47}$ $Ga_{1.25}Mn_{1.81}$ ($\pm 5\%$). Seven crystallites showing a high degree of crystallinity were studied in detail by ED. A reciprocal lattice was constructed, and diffraction patterns taken along various zone axes could be indexed in space group $Pcm2_1$ with $a \sim 5.4$ Å, $b \sim 11.4$ Å and $c \sim 5.3$ Å. Lattice images could be well matched to computer simulations based on the structural parameters derived from our neutron diffraction experiments. Again, there was no evidence for the presence of microdomains showing a doubling of the unit cell along [010].

The temperature dependence of the molar magnetic susceptibility of $Ca_{2.5}Sr_{0.5}Ga_{1.2}Mn_{1.8}O_8$ is shown in Fig. 12. The data show a broad maximum in the temperature range $150 \leqslant T(K) \leqslant 300$ and the ZFC and FC data show hysteresis below 150 K. The weak temperature dependence of the data above 150 K renders a description in terms of the Curie–Weiss law inappropriate. The field dependence of the magnetisation at 200, 100 and 5 K is shown in Fig. 13. At 200 K $M(H)$ is a reversible linear function that passes through the origin, but at 100 K hysteresis is present and the function is shifted along the positive magnetisation axis; this displacement is also apparent at 5 K.

Structure refinement using the neutron diffraction data was more straightforward in the case of $Ca_{2.5}Sr_{0.5}Ga_{1.2}Mn_{1.8}O_8$ than in that of the Co-containing composition. The excess Ga was found to be randomly distributed over 10% of the 6-coordinate sites, the remainder being occupied by Mn, and there was no evidence of disorder around the 4-coordinate sites, which were occupied only by Ga. The analysis of the neutron diffraction data collected as a function of temperature thus proceeded smoothly using the same models for the crystal and magnetic structures as were used in the case of $Ca_{2.5}Sr_{0.5}GaMn_2O_8$. The atomic coordinates refined at 270 K and listed in Table 2 can be used to define the structural model. Fig. 14 shows some of the changes that occur in the diffraction pattern over the temperature range $140 \leqslant T(K) \leqslant 200$. As the sample is cooled from 200 to 180 K, there is an increase

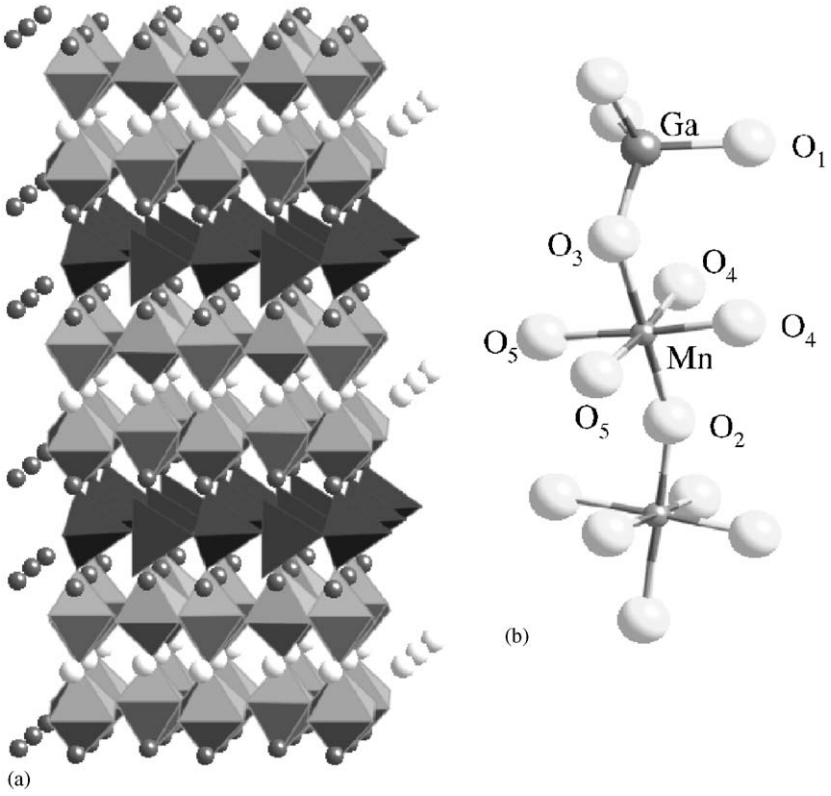

Fig. 5. Crystal structure of $Ca_{2.5}Sr_{0.5}GaCo_{0.15}Mn_{1.85}O_8$. (a) Polyhedral representation with octahedra and tetrahedra shaded light and dark, respectively. Light circles represent Ca/Sr cations, dark circles Ca only. (b) Local coordination around the 6-coordinate and 4-coordinate sites (ordered model).

in the diffuse scattering at a *d*-spacing of ~5.4 Å. At 150 K this scattering can arguably be described as the sum of two weak Bragg peaks, and at 140 K two Bragg peaks are clearly present. Although it is not physically meaningful, the intensity of the diffuse scattering was such that it was possible to include an ordered magnetic moment in the structural model for $T \leqslant 190\,K$; the temperature dependence of the ordered moment over the range $80 \leqslant T(\mathrm{K}) \leqslant 220$ is shown in Fig. 15; a saturation value of 3.17(5) μ_B was determined from the data collected at 10 K. The unit cell parameters *a* and *c* show (Fig. 16) no anomaly at 150 K, but parameter *b* shows a broad minimum for $130 \leqslant T(\mathrm{K}) \leqslant 170$ and then increases on cooling between 130 and 100 K; the unit cell volume consequently increases on cooling through the temperature range $100 \leqslant T(\mathrm{K}) \leqslant 130$. The bond lengths around the 6-coordinate site do not show any significant change at the Néel temperature, and neither does the Mn–O2–Mn bond angle (Fig. 17). Fig. 18 shows that, as in the case of $Ca_{2.5}Sr_{0.5}GaCo_{0.15}Mn_{1.85}O_8$, the bond lengths around the 4-coordinate site do not show a significant response to the magnetic phase transition.

4. Discussion

The difference between the behaviour of $Ca_{2.5}Sr_{0.5}GaCo_{0.15}Mn_{1.85}O_8$ and that of $Ca_{2.5}Sr_{0.5}GaMn_2O_8$ is remarkable. Our decision to synthesise the former material was driven by a desire to vary the Mn^{3+}:Mn^{4+} ratio away from the value of unity found in the undoped material. We anticipated that, if it entered the structure, the dopant would do so on the 6-coordinate sites as Co^{3+}. However, our refinements of the site occupancies and the magnetic structure both show that substitution takes place at the 4-coordinate site, with the displaced Ga^{3+} cations moving to the octahedral sites. The resultant disorder may be the reason that the displacement parameter of O3, which is linked to both sites, is always higher than those of O4 and O5, which are only linked to 6-coordinate sites. The presence of a random distribution of 15% Co and 85% Ga on the tetrahedral sites provides an explanation for the structural disorder observed on the O1 sublattice; a similar effect was observed in $Sr_2Co_{1.2}Ga_{0.8}O_5$ [13] which also shows Co/Ga disorder on a 4-coordinate site. The preference for the tetrahedral site perhaps raises a question concerning the oxidation state of the Co, given that Co^{2+} is often found in this geometry. However, in the brownmillerite $Sr_2Co_2O_5$, high-spin Co^{3+} cations occupy both the octahedral and tetrahedral sites. When 50% of the Co is replaced by Fe^{3+} in Sr_2FeCoO_5, partial cation ordering (57:43) occurs on prolonged annealing, with the Co^{3+} cations having a preference for the tetrahedral sites [14,15]. The size match between Ga^{3+} and Co^{3+} is also better than that with Co^{2+}, and these arguments together

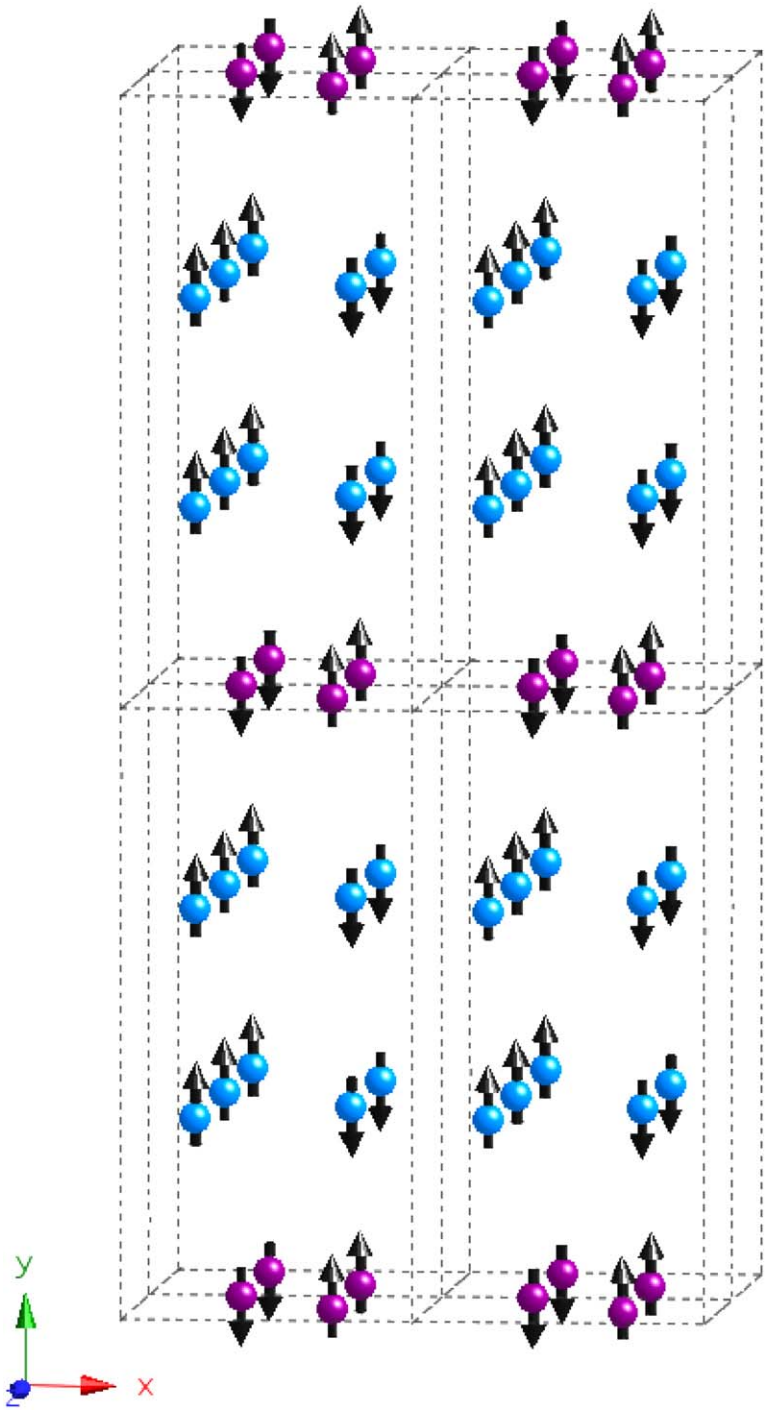

Fig. 6. Magnetic structure of $Ca_{2.5}Sr_{0.5}GaCo_{0.15}Mn_{1.85}O_8$.

lead us to conclude that the dopant enters the tetrahedral sites as Co^{3+}. The distribution of cations and oxidation states over the two octahedral sites in the formula unit is then 0.15 Ga^{3+}, 0.85 Mn^{3+} and 1.0 Mn^{4+}. This surprising distribution of cations might be linked to the extreme difficulty we experienced when attempting to cation-dope the parent phase. The range of Mn–O bond lengths in the MnO_6 octahedra can be parameterised using the distortion parameter

$$\sigma_{JT} = \sqrt{\frac{1}{6}\sum_i [(Mn-O)_i - \langle Mn-O\rangle]^2},$$

which takes a value of 0.086 at 300 K. This is smaller than the value observed in $Ca_{2.5}Sr_{0.5}GaMn_2O_8$, as is to be expected given the reduction in the fraction of the sites

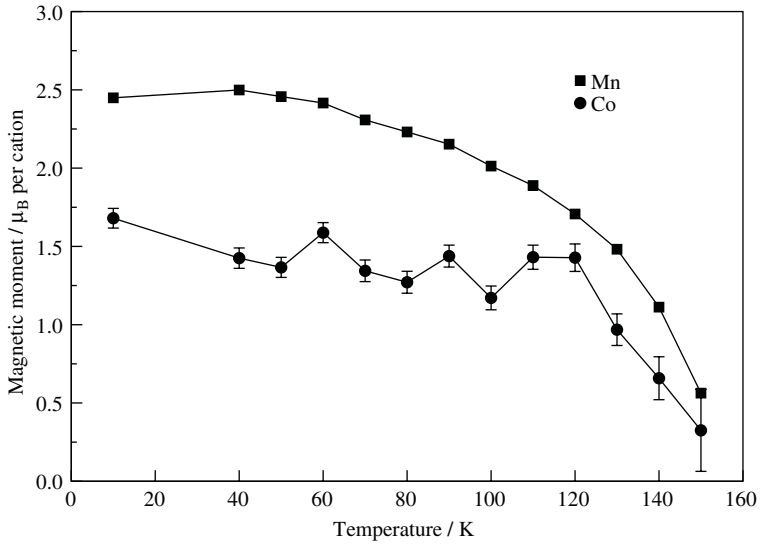

Fig. 7. Temperature dependence of the ordered magnetic moment at the Mn and Co sites in $Ca_{2.5}Sr_{0.5}GaCo_{0.15}Mn_{1.85}O_8$.

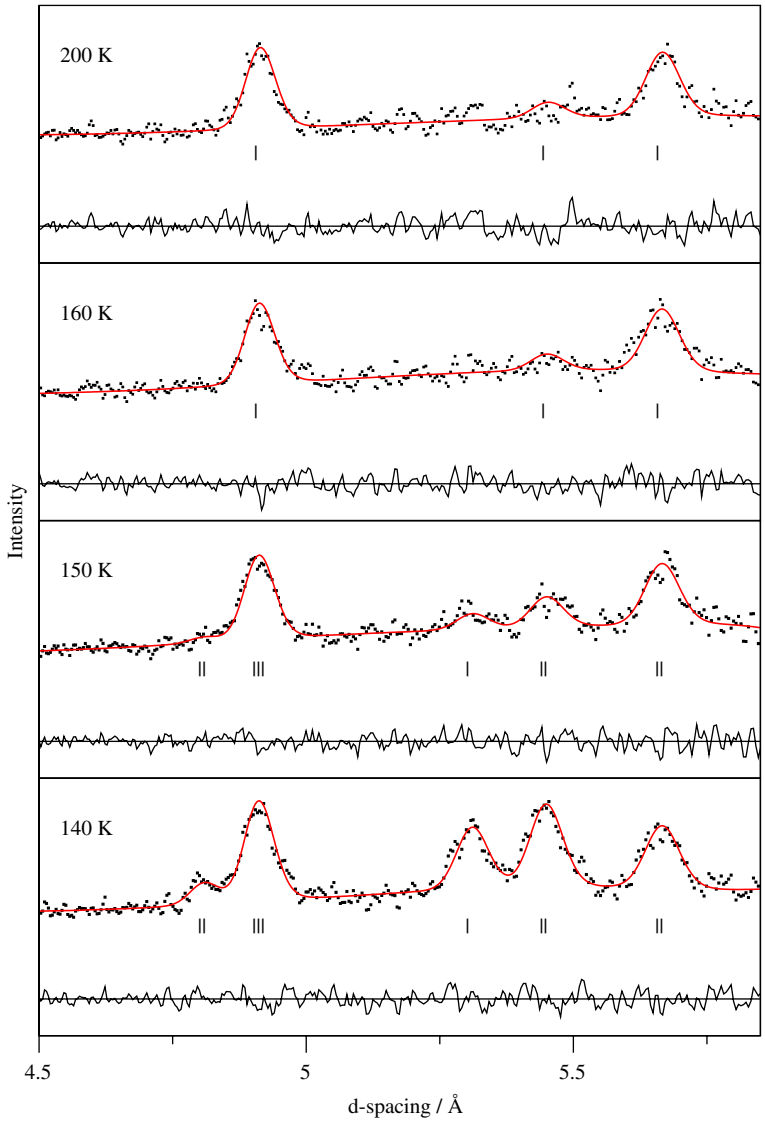

Fig. 8. Temperature dependence of the neutron powder diffraction profile of $Ca_{2.5}Sr_{0.5}GaCo_{0.15}Mn_{1.85}O_8$ in the *d*-spacing region where magnetic scattering is strongest.

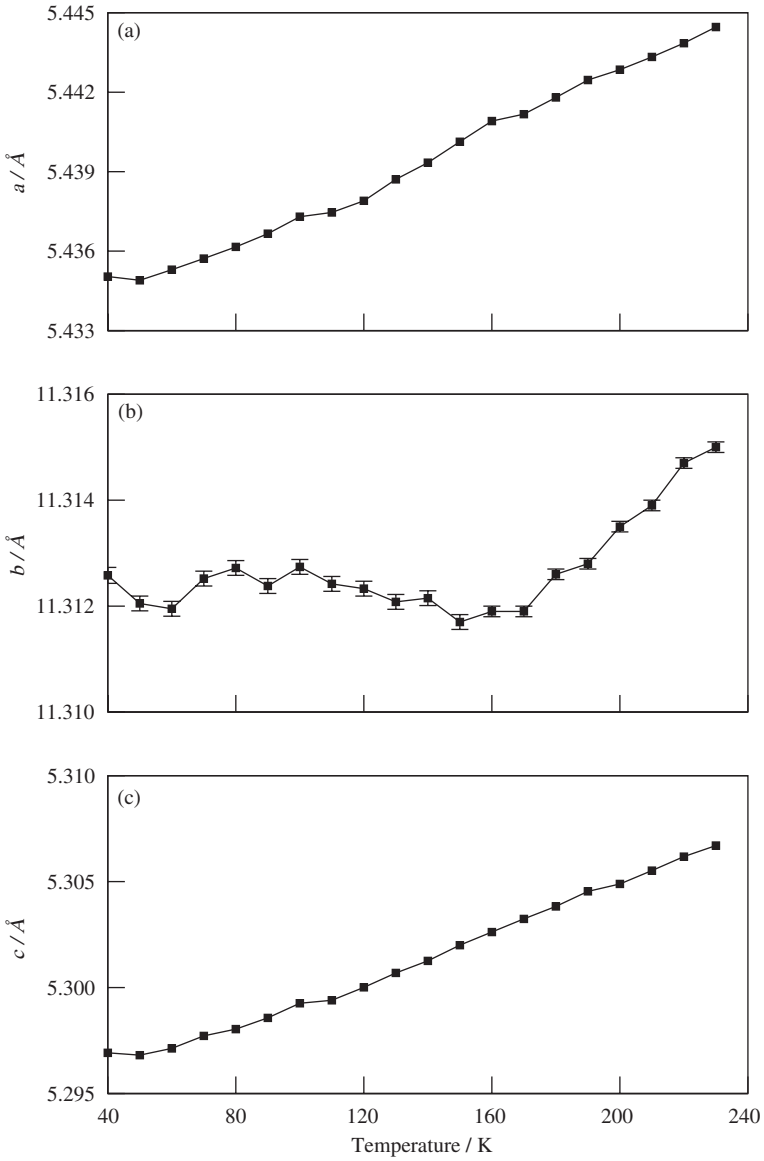

Fig. 9. Temperature dependence of the unit cell parameters of $Ca_{2.5}Sr_{0.5}GaCo_{0.15}Mn_{1.85}O_8$.

occupied by Jahn-Teller active Mn^{3+} cations. There are changes in the shape of the octahedra, although Mn–O3 remains the longest bond. The principal difference between the octahedral sites in the two compositions is that the two crystallographically inequivalent Mn–O4 bond lengths in $Ca_{2.5}Sr_{0.5}GaMn_2O_8$ are significantly different, whereas in the Co-doped sample they are essentially equal; the same is true of the Mn–O5 bonds. The mean Mn–O4 bond length is the same in the two compounds whereas the mean Mn–O5 distance is shorter in the original composition; the former bonds are always longer than the latter. A further striking structural change at the atomic scale at 300 K is that the lengths of the two inequivalent Ga/Co–O1 bonds are significantly different in $Ca_{2.5}Sr_{0.5}GaCo_{0.15}Mn_{1.85}O_8$, whereas they are essentially equal in $Ca_{2.5}Sr_{0.5}GaMn_2O_8$. Structural changes do not only occur at the atomic level. Domains in which there was a doubling of the periodicity along the *y*-axis were observed in the microstructure of the parent compound but not in that of the doped material; these extended defects were attributed to an ordering of different orientations of the GaO_4 tetrahedra. The substitution of Co onto the 4-coordinate site and the concomitant transfer of Ga to the 6-coordinate site thus have a marked effect on the chemical bonding within each octahedral and tetrahedral layer and on the long-range stacking of the latter.

The temperature dependence of the magnetic susceptibility of $Ca_{2.5}Sr_{0.5}GaCo_{0.15}Mn_{1.85}O_8$ is very different to that observed in the case of $Ca_{2.5}Sr_{0.5}GaMn_2O_8$. Whereas the latter shows a broad maximum at ~200 K, ~50 K above the Néel temperature, the former shows a well-defined transition at 155 K, coincident, within error,

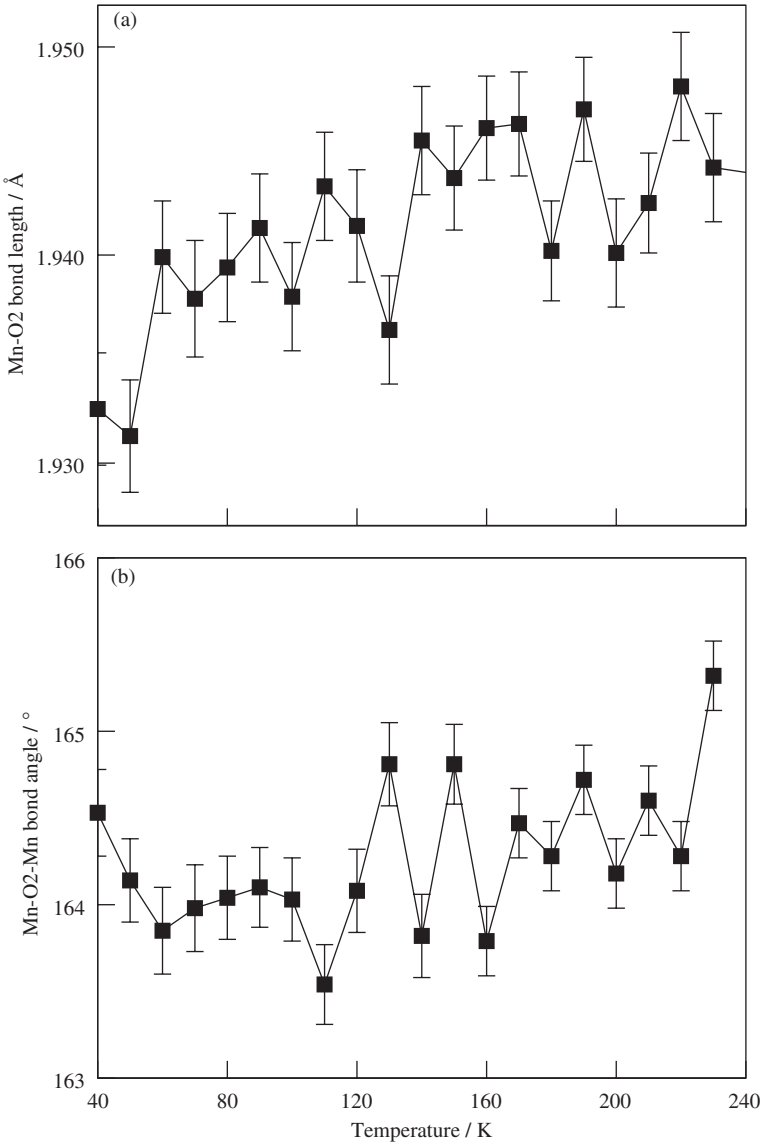

Fig. 10. Temperature dependence of the Mn–O2 bond lengths and Mn–O2–Mn bond angles in $Ca_{2.5}Sr_{0.5}GaCo_{0.15}Mn_{1.85}O_8$.

with the temperature at which the onset of long-range magnetic ordering was detected by neutron diffraction. In the case of $Ca_{2.5}Sr_{0.5}GaMn_2O_8$, the true Néel temperature (T_N) could not be identified from the susceptibility data. The change in $\chi(T)$ is evidence that the extensive short-range magnetic ordering that occurs above T_N within the perovskite bilayers of the undoped compound is not reproduced in $Ca_{2.5}Sr_{0.5}GaCo_{0.15}Mn_{1.85}O_8$. The absence, at temperatures just above T_N, of diffuse scattering at a *d*-spacing of $\sim$5.4 Å in the neutron diffraction pattern is further evidence for the absence of significant short-range order. The Weiss constant (−238 K) derived from a fit to the Curie–Weiss law is reasonable for an antiferromagnet with $T_N = 155$ K, although the Curie constant is somewhat larger than the value predicted by the spin-only formula (4.875 emu). The behaviour of $\chi(T)$ below T_N is more unusual; the ZFC and FC data no longer overlie, with the former increasing more rapidly on cooling. The Mn cations clearly order in an antiferromagnetic structure similar to that of $Ca_{2.5}Sr_{0.5}GaMn_2O_8$, thus forming ferromagnetic [010] chains. We propose that the *y* spin component of the Co^{3+} cations located within the tetrahedral layers is coupled into these chains by antiferromagnetic super-exchange with neighbouring Mn cations, but the structural disorder causes the transverse *x* and *z* components to remain disordered until they freeze into a spin-glass state at $\sim$10 K. The difference between the ZFC and FC data observed below 150 K can then be attributed to the blocking of spins above the glass-transition temperature, possibly caused by the interaction of the disordered spin components with the internal magnetic field. This model is consistent with the low value of the ordered magnetic

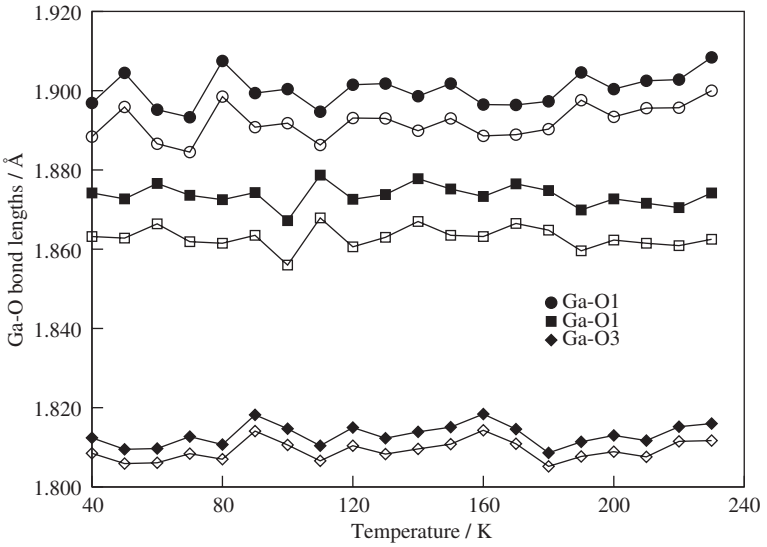

Fig. 11. Temperature dependence of the Ga–O1 and Ga–O3 bond lengths in $Ca_{2.5}Sr_{0.5}GaCo_{0.15}Mn_{1.85}O_8$. Filled (hollow) symbols relate to a model in which O1 is disordered (ordered).

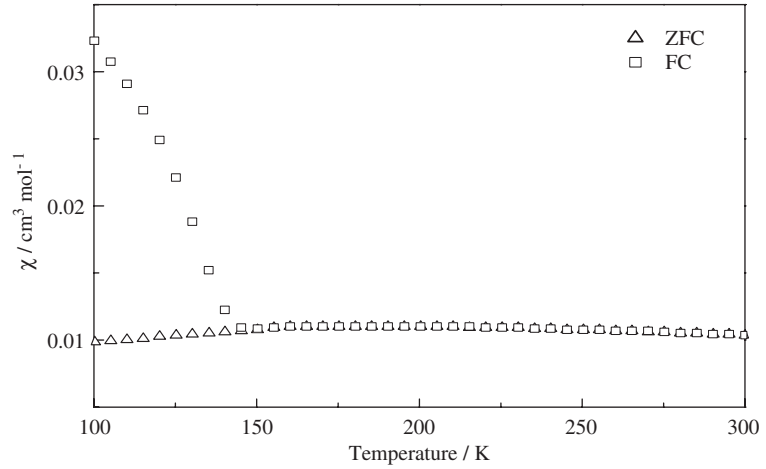

Fig. 12. Temperature dependence of the molar magnetic susceptibility of $Ca_{2.5}Sr_{0.5}Ga_{1.2}Mn_{1.8}O_8$ measured in 100 Oe after zero-field cooling (ZFC) and field cooling (FC).

moment observed on the Co^{3+} cations, and with the displaced hysteresis loop observed at 5 K. Although the magnetic properties of the Co-doped composition differ from those of the parent compound in many ways, the presence of Ga^{3+} on 7.5% of the 6-coordinate sites and Co^{3+} on 15% of the 4-coordinate sites is not enough to modify the long-range antiferromagnetic structure adopted at low temperatures within the bilayers. In view of the low Ga^{3+} concentration it is not surprising that the π superexchange interactions are strong enough to maintain the antiferromagnetic ordering within the individual perovskite sheets of the bilayers. It is more noteworthy, given that the introduction of Ga^{3+} will specifically reduce the concentration of Mn^{3+} cations, that the ferromagnetic superexchange along [010], which stems from the presence of partially occupied e_g orbitals on Mn^{3+} cations, is maintained. However, the retention of the elongation of the Mn–O3 bond and, to a lesser extent, the Mn–O2 bond ensures that the appropriate d orbital is occupied, and that ferromagnetic coupling of neighbouring Mn^{3+}/Mn^{4+} cations is favoured along the *y*-axis. The mean value of the ordered magnetic moment of a Mn cation (2.45 μ_B) is lower than the value found in the parent compound (3.09 μ_B) as is to be expected given the reduction in the concentration of the magnetic Mn^{3+} cations. However, the size of the reduction is perhaps larger than might have been expected, suggesting that some Mn cations, presumably those with the most Ga neighbours,

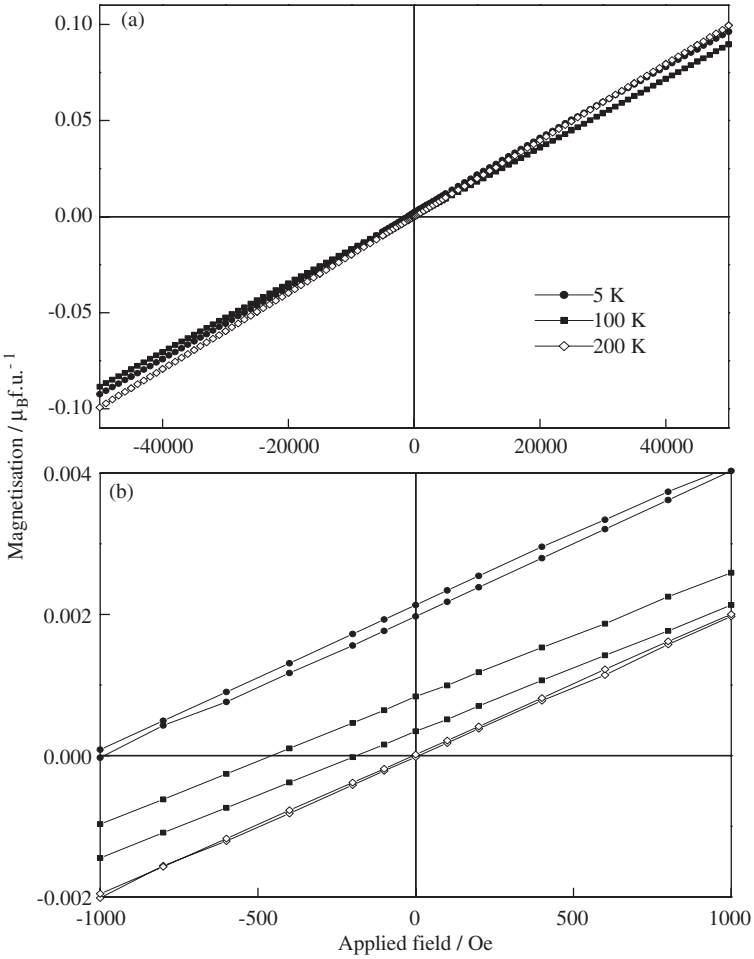

Fig. 13. Field dependence of the magnetisation of $Ca_{2.5}Sr_{0.5}Ga_{1.2}Mn_{1.8}O_8$ at selected temperatures.

Table 2
Structural parameters of $Ca_{2.5}Sr_{0.5}Ga_{0.2}Mn_{1.8}O_8$ at 270 K

Atom	x	y	z	Uiso (Å^2)
Ca	0.2261(3)	0.1880(1)	0.5134(7)	0.0070(2)
Ca/Sr[a]	0.2408(3)	0.5	0.4947(7)	0.0064(4)
Mn/Ga[b]	0.2581(2)	0.3306(1)	0	0.0036(7)
Ga	0.3204(2)	0	0.0534(7)	0.0029(5)
O1	0.3660(3)	0	0.4082(7)	0.0036(5)
O2	0.3033(3)	0.5	−0.001(1)	0.0108(4)
O3	0.1873(2)	0.1425(1)	−0.0216(8)	0.0038(3)
O4	−0.0027(3)	0.3432(1)	0.2452(9)	0.0022(2)
O5	0.4920(3)	0.3072(1)	0.2591(8)	0.0033(3)

Space group $Pcm2_1$, $a = 5.4411(3)$, $b = 11.3823(6)$, $c = 5.3063(3)$ Å; $R_{wp} = 4.65\%$, $\chi^2 = 2.25$.
[a]Random distribution in a 1:1 ratio.
[b]Random distribution in a 9:1 ratio.

contribute to the spin-glass component of the magnetism, rather than to the antiferromagnetic component.

The temperature dependence of the structural chemistry of $Ca_{2.5}Sr_{0.5}GaCo_{0.15}Mn_{1.85}O_8$ shows both similarities and differences to that of $Ca_{2.5}Sr_{0.5}GaMn_2O_8$. In both cases the unit cell parameters a and c decrease smoothly through the temperature range studied, whereas b, representing the periodicity of the structure perpendicular to the layers, shows a negative temperature gradient close to T_N. The minimum in b is broader in the case of the undoped sample. However, the clear correlations between bond lengths and magnetic ordering that were identified in the case of $Ca_{2.5}Sr_{0.5}GaMn_2O_8$ are not apparent in the Co-containing composition. The difference is most striking in the case of the bond lengths around the 4-coordinate site, but it is also apparent in those of the Mn–O2–Mn bond angle and, for example, the Mn–O4 bond lengths. In the absence of structural changes in the region of T_N, the retention of ferromagnetic coupling between Mn cations along [010] provides the strongest evidence that one-dimensional charge ordering of Mn^{3+} and Mn^{4+} is maintained when $Ca_{2.5}Sr_{0.5}GaMn_2O_8$ is Co-doped.

The above discussion details the changes in the structural chemistry and magnetic properties that occur when $Ca_{2.5}Sr_{0.5}GaMn_2O_8$ is doped with Co. However, it is not clear to what extent the cause of the behavioural changes lies in the presence of diamagnetic Ga on the 6-coordinate site, as against the presence of magnetic Co on the 4-coordinate site. We hoped to be able to decouple these two factors by studying $Ca_{2.5}Sr_{0.5}Ga_{1.2}Mn_{1.8}O_8$ in which the 6-coordinate sites are again partially occupied by Ga, but

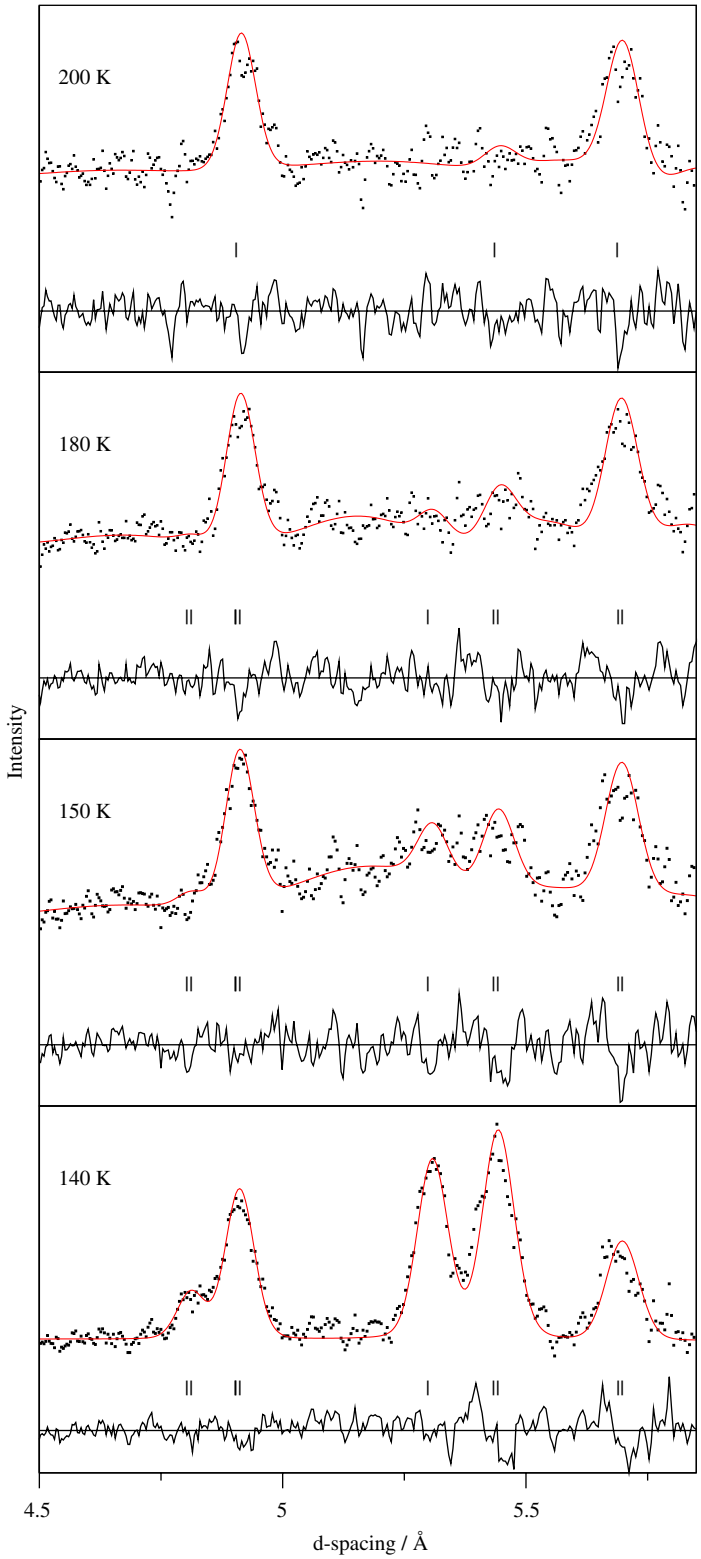

Fig. 14. Temperature dependence of the neutron powder diffraction profile of $Ca_{2.5}Sr_{0.5}Ga_{1.2}Mn_{1.8}O_8$ in the *d*-spacing region where magnetic scattering is observed.

the 4-coordinate sites do not contain any magnetic cations. We were able to refine the structure of the Ga-rich phase without introducing disorder into the tetrahedral layers. This is unsurprising, and supports the proposal that the disorder in the Co-containing phase stems from the different coordination requirements of Co^{3+} and Ga^{3+}. As in the case of $Ca_{2.5}Sr_{0.5}GaCo_{0.15}Mn_{1.85}O_8$, the two Ga–O1 bond lengths around the tetrahedral site are

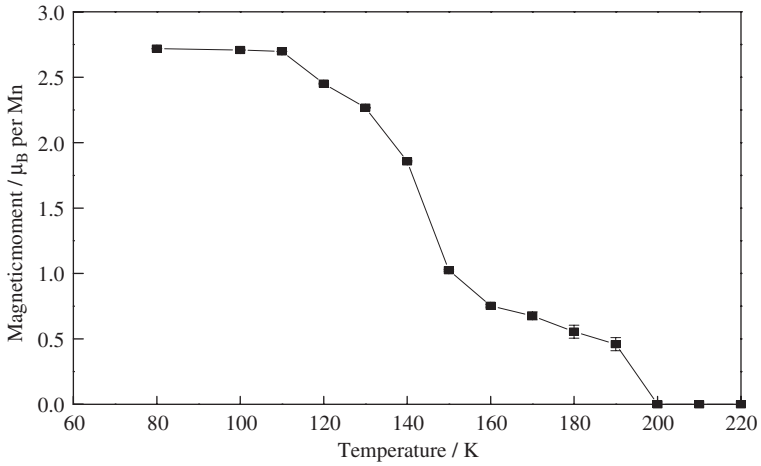

Fig. 15. Temperature dependence of the ordered magnetic moment at the Mn sites in $Ca_{2.5}Sr_{0.5}Ga_{1.2}Mn_{1.8}O_8$.

significantly different. This is the first clear evidence that chemical changes at the 6-coordinate site can have a marked effect on the 4-coordinate site in this group of compounds. The distortion parameter takes the value $\sigma_{JT} = 0.096$ at 270 K, not significantly different from the parent compound. However, as in the case of the Co-substituted material, the difference between the two Mn–O4 and Mn–O5 bond lengths is markedly reduced in the Ga-rich composition, by ~50% and ~80%, respectively.

The temperature dependence of the magnetic susceptibility of $Ca_{2.5}Sr_{0.5}Ga_{1.2}Mn_{1.8}O_8$ bears a strong similarity to that of the parent compound. The relatively small variation in $\chi(T)$ for $150 \leqslant T(K) \leqslant 300$ suggests that the presence of Ga^{3+} on 10% of the cation sites within the bilayers is not enough to prevent extensive short-range magnetic ordering, and this is consistent with the appearance of diffuse scattering in the neutron diffraction pattern some 30 K above T_N. The diffuse scattering was not observed in the case of $Ca_{2.5}Sr_{0.5}GaCo_{0.15}Mn_{1.85}O_8$, in which only 7.5% of the octahedral sites is occupied by Ga^{3+}. The saturation value of the ordered Mn moment at 10 K is similar to that found in the parent compound, also in contrast to the Co-doped compound, suggesting that the introduction of Ga onto the 6-coordinate sites does not interfere significantly with the establishment of long-range magnetic order. These observations show that the presence of magnetic Co^{3+} on 15% of the tetrahedral sites is largely responsible for the disruption of the magnetic coupling within the bilayers in $Ca_{2.5}Sr_{0.5}GaCo_{0.15}Mn_{1.85}O_8$. The link between the two cation sublattices in these compounds is clearly too strong for them ever to be considered as independent, either structurally or magnetically. One aspect of the magnetic data shown in Fig. 12 deserves further comment. In our original study of $Ca_{2.5}Sr_{0.5}GaMn_2O_8$, we showed that the FC susceptibility increased on cooling below 125 K. We ascribed this to the canted spin structure of a low-level perovskite impurity that could be seen in the diffraction pattern recorded at 5 K. In the present case the rise in the FC susceptibility coincides with the appearance of magnetic Bragg peaks in the diffraction pattern of the principal phase. No impurity phase could be seen in diffraction patterns of $Ca_{2.5}Sr_{0.5}Ga_{1.2}Mn_{1.8}O_8$ collected at 100 K, and it is therefore likely that the rise in the susceptibility is associated with the principal phase. The modest magnitude of the rise, together with the displaced hysteresis in $M(H)$ at 100 K suggests that a glassy magnetic component is present, although comparison of Figs. 4 and 13 shows that is less significant than in the Co-doped phase. It is perhaps attributable to a low density of decoupled Mn cations. This raises the possibility that the parent compound orders antiferromagnetically at 150 K, and then under goes a re-entrant transition at 125 K, the temperature at which the resistivity shows a marked change. If this interpretation
is correct it should be possible to use neutron diffraction to locate a magnetic phase transition in the perovskite impurity in the temperature range $5 \leqslant T(K) < 125$. In order to resolve this issue, further experiments designed to study both the parent compound and the Ga-rich composition at temperatures below 100 K are planned; they will be reported at a later date.

The response of the unit cell parameter b of $Ca_{2.5}Sr_{0.5}Ga_{1.2}Mn_{1.8}O_8$ to the onset of magnetic ordering occurs over a wide temperature range and thus resembles that of the parent compound more closely than it resembles that of $Ca_{2.5}Sr_{0.5}GaCo_{0.15}Mn_{1.85}O_8$. This is consistent with the presence of short-range ordering in all but the latter material. However, the clear link between the magnetic phase transition and the lengths of specific bonds, at both the octahedral and tetrahedral sites, that was apparent in the parent compound but absent in the Co-substituted material is also absent in the case of the Ga-rich composition. This is presumably because the structural modifications that facilitate doping with excess Ga at high

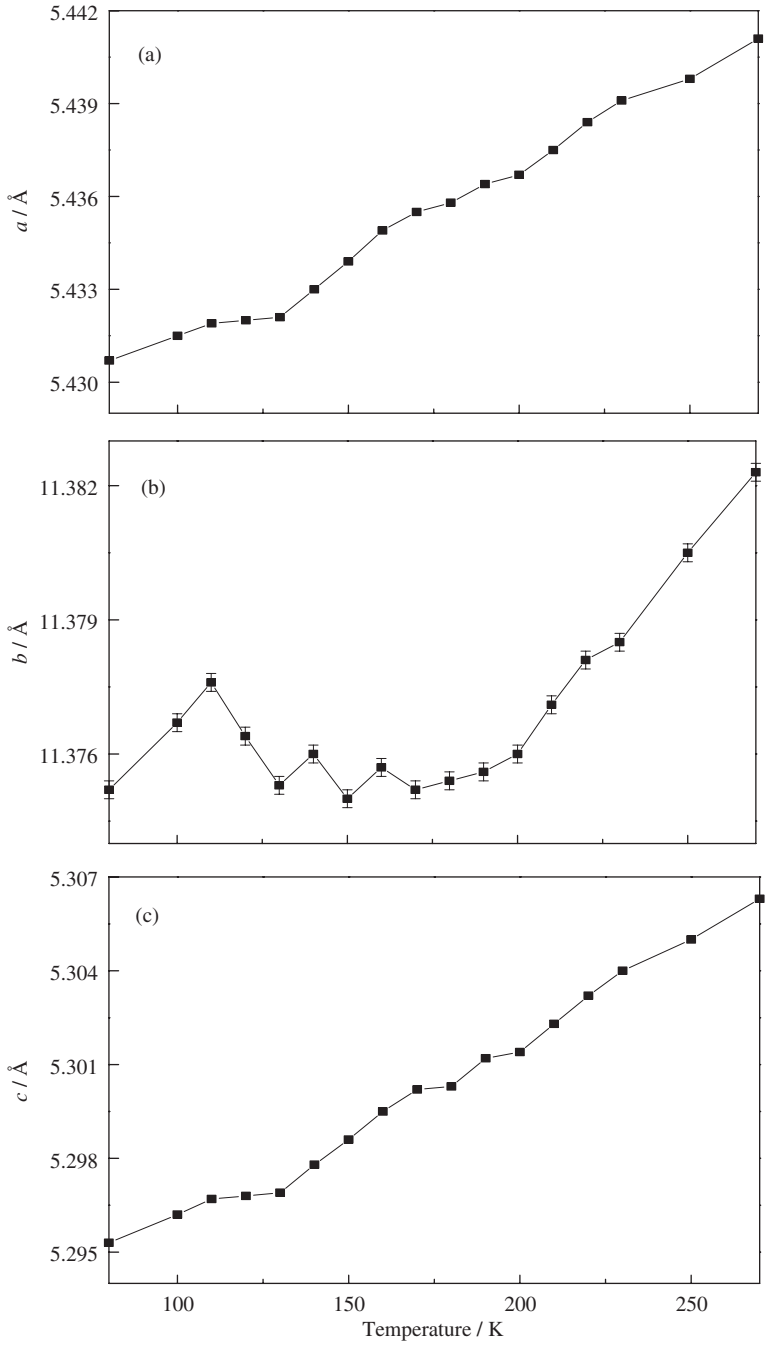

Fig. 16. Temperature dependence of the unit cell parameters and unit cell volume of $Ca_{2.5}Sr_{0.5}Ga_{1.2}Mn_{1.8}O_8$.

temperatures, for example, the loss of the degeneracy of the Ga–O1 bond lengths, removes the possibility of a coherent response to the onset of magnetic ordering. The structural changes at the 4-coordinate site caused by the chemical substitution are those that are required to accommodate the magnetic ordering and the magnetic structure is thus to some extent pre-formed. It is again apparent that the introduction of Ga onto the 6-coordinate sites, with the occupation of the 4-coordinate sites unaltered, is enough to produce significant changes in the structural behaviour of these systems. This comment is applicable not just to the local structure but also to the microstructure, as is demonstrated by the results of our electron microscopy experiments. Only in the case of the parent compound do we see microdomains which can be associated with changes in the orientation of the GaO_4 tetrahedra. We cannot rule out the possibility that the absence of these microdomains from the compositions described above is

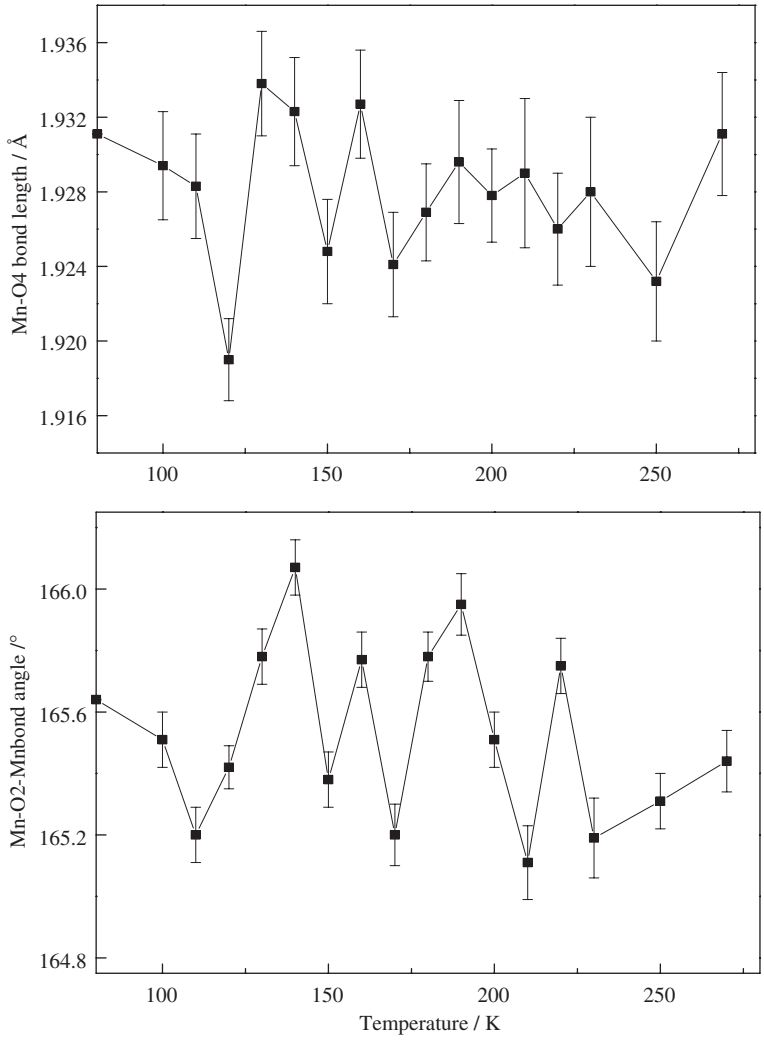

Fig. 17. Temperature dependence of Mn–O4 bond lengths and Mn–O2–Mn bond angles in $Ca_{2.5}Sr_{0.5}Ga_{1.2}Mn_{1.8}O_8$.

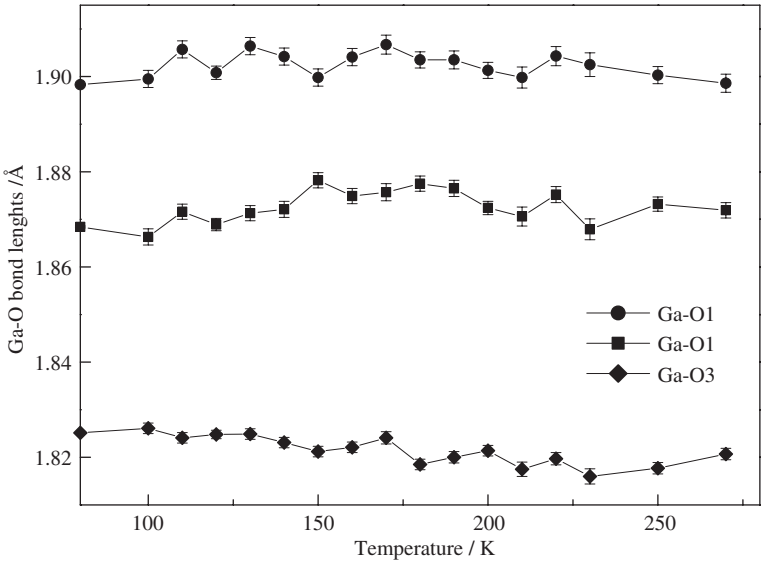

Fig. 18. Temperature dependence of the Ga–O1 and Ga–O3 bond lengths in $Ca_{2.5}Sr_{0.5}Ga_{1.2}Mn_{1.8}O_8$.

partly responsible for the changes observed in the magnetic properties.

Acknowledgments

R.R.B. and M.A. acknowledge the financial support provided through the Human Potential Program of the European Community under contract HPRN-CT-2002-00293 [SCOOTMO]. P.P.C.F. acknowledges the award of an EPSRC studentship. We also acknowledge the experimental assistance provided by staff at the ISIS facility.

References

[1] P.D. Battle, S.J. Blundell, P.N. Santhosh, M.J. Rosseinsky, C. Steer, J. Phys: Condens. Matter 14 (2002) 13569.
[2] P.D. Battle, S.J. Blundell, M.L. Brooks, M. Hervieu, C. Kapusta, T. Lancaster, S.P. Nair, C.J. Oates, F.L. Pratt, M.J. Rosseinsky, et al., J. Am. Chem. Soc. 126 (2004) 12517.
[3] G.R. Blake, L. Chapon, P.G. Radaelli, D.N. Argyriou, M.J. Gutmann, J.F. Mitchell, Phys. Rev. B 66 (2002) 144412.
[4] A. Daoud-Aladine, J. Rodriguez-Carvajal, L. Pinsard-Gaudart, M.T. Fernandez-Diaz, A. Revcolevschi, Phys. Rev. Lett. 89 (2002) 097205.
[5] M. Hervieu, S. Malo, O. Perez, P. Beran, C. Martin, G. Baldinozzi, B. Raveau, Chem. Mater. 15 (2003) 523.
[6] M. Ibarra, R. Retoux, M. Hervieu, C. Autret, A. Maignan, C. Martin, B. Raveau, J. Solid State Chem. 170 (2003) 361.
[7] T. Kimura, T. Goto, H. Shintani, K. Ishizaka, T. Arima, Y. Tokura, Nature 426 (2003) 55.
[8] P.G. Radaelli, D.E. Cox, L. Capogna, S.W. Cheong, M. Marezio, Phys. Rev. B 59 (1999) 14440.
[9] P.A. Stadelman, Ultramicroscopy 21 (1987) 131.
[10] A.C. Larson, R.B. von-Dreele, General Structure Analysis System (GSAS), Los Alamos National Laboratories, Report LAUR 86-748, 1990.
[11] P.D. Battle, M.A. Green, J. Lago, J.E. Millburn, M.J. Rosseinsky, J.F. Vente, Chem. Mater. 10 (1998) 658.
[12] P.D. Battle, W.R. Branford, A. Mihut, M.J. Rosseinsky, J. Singleton, J. Sloan, L.E. Spring, J.F. Vente, Chem. Mater. 11 (1999) 674.
[13] F. Lindberg, S.Y. Istomin, P. Berastegui, G. Svenson, S.M. Kazakov, E.V. Antipov, J. Solid State Chem. 173 (2003) 395.
[14] P.D. Battle, T.C. Gibb, P. Lightfoot, J. Solid State Chem. 76 (1988) 334.
[15] P.D. Battle, T.C. Gibb, S. Nixon, J. Solid State Chem. 73 (1988) 330.